

CHALMERS



Effects of Phase Discontinuity due to Power Amplifiers on a WCDMA Uplink

Master's Thesis in Communication Engineering

Shijia Liu

Department of Signals & Systems
CHALMERS UNIVERSITY OF TECHNOLOGY
Gothenburg, Sweden 2015
Master's Thesis 2015:1

MASTER'S THESIS

**Effects of Phase Discontinuity due to
Power Amplifiers on a WCDMA Uplink**

Authors:

Andreas Theodorakopoulos
Lund University

Shijia Liu
Chalmers University of Technology

February 20, 2015

Abstract

The major objective of this study is to identify and understand the way that a power amplifier affects a signal at a WCDMA uplink. More specifically, the phase distortion that is produced when a signal enters the power amplifier in order to get amplified and then sent over a channel. An end-to-end link simulator is built in order to come as close as possible to a realistic system. Furthermore, the phase distortion is modelled and added to the signal in order to finally study the performance of the system in terms of bit error rate.

The study was conducted at Ericsson AB in Gothenburg. Insights about real WCDMA systems were used in order to implement a realistic simulator. The thesis introduces the WCDMA air interface and describes it in terms of the components that were used for the simulations. Matlab was used as the main simulation platform for all the components of the simulated link. The phase distortion was modelled with models that already exist in the literature, and is added to the simulation chain. The study was performed at baseband frequencies. The channel knowledge was assumed to be perfect. For this study only one user was simulated. Results were acquired which showed that the simulated WCDMA air interface system can easily cope with the phase distortion of a typical power amplifier considering QPSK. The distortion that was produced was not able to degrade the robust performance of the system. Based on our simulation results about the power amplifiers that are nowadays used for the uplink user equipments, there should be no need of taking further measures to cope with the phase distortion.

Keywords: WCDMA uplink, G-Rake, phase distortion, power amplifier

Acknowledgements

Firstly, we would like to thank Florent Munier, who has been our supervisor during the first months of our work. He gave us the original idea and the opportunity to acquire important knowledge in the field of telecommunications as well as a very valuable experience at Ericsson. Furthermore, we would like to give many thanks to Anders Hansson who successfully guided us at the second half of the thesis. Last but not least we would like to express our gratitude to Anders Persson for his valuable knowledge about the G-Rake receiver.

Contents

List of Figures	iii
List of Tables	v
List of Abbreviations	vi
List of Symbols	viii
1 Introduction	1
1.1 Background	1
1.2 Problem Description	2
1.3 Scope and Purpose	2
1.4 Limitations	2
1.5 Methodology	2
1.6 Thesis outline	3
2 WCDMA Link Model	4
2.1 Concepts of a WCDMA System	4
2.1.1 WCDMA Background	4
2.1.2 Uplink Physical Channels	5
2.1.3 Main Parameters of WCDMA Uplink	6
2.2 WCDMA Uplink Simulator	7
2.2.1 Digital Modulation	7
2.2.2 Channel Coding	8
2.2.3 WCDMA Codes	8
2.2.4 Pulse Shaping and Matched Filter	11
2.2.5 Multipath Propagation	11
2.2.6 Channel Estimation	12
2.2.7 Receiver Diversity	12
2.3 Power Amplifier Model	14
2.3.1 Saleh Model	15

2.3.2	Polynomial Model	16
3	Distortion Characterisation and Simulation Results	17
3.1	Simulator Implementation	17
3.1.1	WCDMA Configuration	17
3.1.2	SNR Calculation	18
3.1.3	Turbo Coder and Modulation	19
3.1.4	Rayleigh Fading and Multipath Channel Generation	19
3.1.5	Spreading	20
3.1.6	Channel Estimation	22
3.1.7	G-Rake Receiver	23
3.2	PA Distortion Characterisation	24
3.2.1	Saleh Model	24
3.2.2	Polynomial Model	27
3.3	Simulation Results	30
3.3.1	Saleh Results	30
3.3.2	Polynomial Results	33
4	Conclusions	37
	Appendix A RAKE Receiver	39
	Bibliography	43

List of Figures

2.1	The uplink dedicated channel frame structure used in WCDMA	6
2.2	A block diagram of the locally developed WCDMA uplink simulator	7
2.3	QPSK signal constellation with Gray coding.	8
2.4	OVSF codes tree	9
2.5	WCDMA uplink spreading and scrambling functions	10
2.6	WCDMA uplink despreading and descrambling functions	11
2.7	Multipath propagation from base station to user equipment	12
2.8	One realisation of a Rayleigh fading channel caused by multipath propagation (PA3)	12
2.9	RAKE receiver	13
3.1	High speed channel on top of DPDCH and DPCCH. (The HS has 4 times the power of DPDCH/DPCCH, and it has a specific burst pattern as shown.)	18
3.2	SNR definition of the simulator. The red is signal power level which is always fixed to 100% and the blue is noise power percentage which changes according to different SNR in dB compared with unity signal power.	19
3.3	Multipath and tap delays at Pedestrian-A 3 km/h. Each tap comes at a specific delay. The summation provides the multipath signal.	20
3.4	Multipath and each path Rayleigh fading channel. This is one realisation of the taps and the summation(multipath) for a duration of one super frame.	20
3.5	Spreading process in waveform. Red is two bits of data that XORs the spreading code(blue) and result in the transmitted signal(green).	21
3.6	Despreading process in waveform. The received signal (green) is XORed by the spreading code (blue) which results in our data (red).	22
3.7	True channel and estimated channel comparison. One realisation of the estimated channel coefficients for two super frames. The comparison with the true channel gives a reasonable fit.	23
3.8	G-Rake receiver finger placement. A finger is assigned for both red and black place.	24

3.9	Saleh model AM/AM and AM/PM. On the left side lies the output power in dB shown by the blue curve in comparison with input power. The red curve shows the phase distortion which applies for a specific input power.	25
3.10	Saleh model phase distortion distribution. The blue curve is the CDF of input signal's amplitude. The red curve explains the corresponding phase distortion of that input power.	26
3.11	Saleh model constellation rotation after the added PA phase distortion	27
3.12	Polynomial model AM/AM and AM/PM. Typical characteristics of a UE power amplifier. The PA is quite linear for most of the input values.	28
3.13	Polynomial model phase distortion distribution. The blue curve is the CDF of input signal's amplitude. The red curve explains the corresponding phase distortion of that input power.	29
3.14	Polynomial model constellation rotation after the added PA phase distortion	30
3.15	Saleh model performance for DPDCH. The raw BER is before the turbo decoder whereas the BER is the performance after the turbo decoder.	31
3.16	Saleh model performance for DPCCH. The raw BER is before the turbo decoder whereas the BER is the performance after the turbo decoder.	31
3.17	Saleh model received signal constellation rotation. The blue start stands for signal without PA's effect, and the red circle stands for signal with PA's phase distortion.	32
3.18	Saleh model block bit error rate	33
3.19	Polynomial model performance for DPDCH. The raw BER is before the turbo decoder whereas the BER is the performance after the turbo decoder.	33
3.20	Polynomial model performance for DPCCH. The raw BER is before the turbo decoder whereas the BER is the performance after the turbo decoder.	34
3.21	Polynomial model received signal constellation rotation. The blue start stands for signal without PA's effect, and the red circle stands for signal with PA's phase distortion.	35
3.22	Polynomial model block bit error rate	36

List of Tables

2.1	WCDMA uplink main parameters	6
3.1	Saleh model variable values used in our simulator	25

List of Abbreviations

AM/AM	Amplitude Modulation/Amplitude Modulation
AM/PM	Amplitude Modulation/Phase Modulation
ASK	Amplitude Shift Keying
AWGN	Additive White Gaussian Noise
BER	Bit Error Rate
BLER	Block Error Rate
BPSK	Binary Phase Shift Keying
BS	Base Station
BTS	Base Transceiver Station
CDMA	Code Division Multiple Access
CN	Core Network
CDF	Cumulative Distribution Function
DPCCH	Dedicated Physical Control Channel
DPCH	Dedicated Physical Channel
DPDCH	Dedicated Physical Data Channel
DS-CDMA	Direct Sequence Code Division Multiple Access
FDD	Frequency Division Duplex
FSK	Frequency Shift Keying
G-Rake	Generalised RAKE

GSM	Global System for Mobile Communications
HS	High Speed
ISI	Inter Symbol Interference
LOS	Line of Sight
LSE	Least Squares Estimator
MRC	Maximum Ratio Combining
MAI	Multiple Access Interference
OVSF	Orthogonal Variable Spreading Factor
PA	Power Amplifier
PSK	Phase Shift Keying
QAM	Quadrature Amplitude Modulation
QPSK	Quadrature Phase Shift Keying
RAN	Radio Access Network
RC	Raised Cosine
RF	Radio Frequency
RRC	Root Raised Cosine
SF	Spreading Factor
SNR	Signal to Noise Ratio
TDD	Time Division Duplex
TDMA	Time Division Multiple Access
UE	User Equipment
UMTS	Universal Mobile Telecommunications System
UTRA	Universal Terrestrial Radio Access
WCDMA	Wideband Code Division Multiple Access
2G	2nd Generation
3G	3rd Generation
3GPP	3rd Generation Partnership Project
PAPR	Peak-to-average Power Ratio

List of Symbols

α	Parameter in Saleh model
β	Parameter in Saleh model
σ_u	Standard deviation of the noise \mathbf{u}
\mathbf{a}	Coefficient vector of gain conversion polynomial
\mathbf{b}	Coefficient vector of phase conversion polynomial
c	Spreading code
E	Energy
G	Voltage gain
\mathbf{h}_n	True channel
$\hat{\mathbf{h}}_n$	Estimated channel
\mathbf{I}	Identity matrix
k	Number of bits per symbol
m	Symbol
N_0	Power spectral density of noise
R	Turbo code rate
\mathbf{R}_u	Impairment covariance matrix
r	Received signal
s	Transmitted symbol series
t	Time

\mathbf{u}_n	Coloured noise including AWGN plus other interferences
V_{in}	Input voltage
V_{out}	Output voltage
\mathbf{w}_n	Finger weight
$\tilde{x}(t)$	Input signal
$\tilde{y}(t)$	Output signal
\mathbf{y}_n	Received signal after descrambling and despreading
z_n	Finger output

1

Introduction

Wideband Code Division Multiple Access (WCDMA), a standard found in *3rd Generation* (3G) mobile telecommunications networks, is nowadays widely used. Due to the very large market using the standard, the best possible quality should be provided by the industry. Therefore, a small change that might improve the standard performance would also improve the user experience. That in return will be a possible increase on the gains of both the operators as well as the developing industry.

1.1 Background

In any communication systems, a *Radio Frequency* (RF) *Power Amplifier* (PA) is used to increase the power of the signal fed to the transmitter antenna. This function is especially important in WCDMA uplink where UE sends signals to the *Base Station* (BS). As the power limitation in UE's mobile devices and transmitted signal's power attenuation and variation as well as the multipath fading exists, the usage of PA can guarantee sufficient power levels of the transmitted signals. The amplifier is located at the RF stage and thus it is a part of the analogue section of the transceiver. But such amplifiers are not perfect component in realizations and amongst their imperfections, non-linear amplification and phase shifting are well known [1]. In the literature these two issues are known as *Amplitude Modulation/Amplitude Modulation* (AM/AM) and *Amplitude Modulation/Phase Modulation* (AM/PM) conversions [2]. AM/AM refers to the non-linear amplification of the input signal as a function of the input signal amplitude, and AM/PM refers to the phase shift of the output signal as a function of the input signal amplitude.

1.2 Problem Description

In WCDMA systems, the mobile terminal's transmitted signal power level can vary over time, due to changes in allocated power based on variable demands for bit rate, and power control mechanisms. Such variations will cause AM/AM and AM/PM distortion. The expected performance of the link might be degraded since the AM/AM and AM/PM are altering the transmitted signal both in amplitude and phase. In the literature the effects of non-linear distortion has been studied for the *Code Division Multiple Access* (CDMA) systems [3], [4]. More specifically work has been done about the downlink where the power levels are very much higher [5]. The problem that is investigated in this study comprises the WCDMA air interface on a Rayleigh Fading channel for the uplink where the power levels are very much lower in order for the user terminals to be power efficient.

1.3 Scope and Purpose

In the present thesis, the phase distortion due to the power amplifier is studied for a WCDMA uplink. The main objective is to build an end-to-end WCDMA simulator from which the behaviour of the PA on the transmitted signal can be captured. From that behaviour only the phase effects will be analysed. Furthermore, the degradation of the performance will be characterised according to the phase effects. The final results will indicate whether furthermore studies for a possible mitigation should be in need.

1.4 Limitations

For this study the case of one user is implemented and thus in the receiver side there is no possible interferences from other users or even other base stations. Also the user is assumed to be using only QPSK modulation where in reality when close to the base station the user might use 16-QAM also. The last limitation is that the channel estimation is assumed to be perfect while in reality a perfect channel estimation cannot be achieved, and that is the main reason it is an estimation.

1.5 Methodology

Matlab is used to build our WCDMA simulation platform. The studied uplink model consists of

- Bit source
- Turbo coding
- *Quadrature Phase Shift Keying* (QPSK) modulation
- Spreading and scrambling
- Oversampling
- *Root Raised Cosine* (RRC) filters
- Power amplifier

- Multipath Rayleigh fading channel
- *Generalised RAKE* (G-Rake) receiver

Figure 2.2 shows the structure of our WCDMA uplink model.

1.6 Thesis outline

Chapter 1 introduces the topic to the reader. Chapter 2 describes in detail the WCDMA physical layer and the architecture of our simulator and we provide the basic theory of PA distortion. In Chapter 3 we characterise the AM/PM distortion using the Saleh model and a polynomial model. Furthermore, we discuss the simulation results. Finally, Chapter 4 provides conclusions and some suggestions for the future work.

2

WCDMA Link Model

This chapter introduces the principles of the WCDMA physical layer (Layer 1) and describes how we build our WCDMA link simulator. The Layer 1 frame structure and main parameters are described in Section 2.1. In Section 2.2, we introduce the concept of turbo coding, spreading and despreading, multipath radio channel, RAKE and G-Rake receiver.

2.1 Concepts of a WCDMA System

Universal Mobile Telecommunications System (UMTS) is a 3G mobile cellular system which emerge after the *Global System for Mobile Communications* (GSM) standard and it is developed, and maintained by the *3rd Generation Partnership Project* (3GPP). UMTS uses WCDMA radio access technology to offer higher spectral efficiency and broader bandwidth, to mobile network operators, than GSM.

Several different terrestrial air interfaces are also provided by UMTS and were named *UMTS Terrestrial Radio Access* (UTRA) at earlier times, but then 'Universal' was kept instead of the whole 'UMTS' as in *Universal Terrestrial Radio Access* (UTRA) to make it more internationally accepted. The architecture of *Radio Access Network* (RAN) includes *User Equipment* (UE), *Core Network* (CN), and BS. UE can be mobile phones and other wireless connected devices. CN is the central part of a telecommunication network that provides various services to customers who are connected by the access network. BS is responsible for handling connections to and from the UEs [6].

2.1.1 WCDMA Background

WCDMA is an access technology used for 3G mobile telecommunications networks. WCDMA provides a variety of services such as voice and multimedia mobile communication services. The organisation that is responsible about the standardisation of WCDMA is 3GPP and it is a composition of various other development organisations [7].

WCDMA uses the *Direct Sequence Code Division Multiple Access* (DS-CDMA) as channel access method and the *Frequency Division Duplex* (FDD) as its basic duplexing method to achieve higher rates and support more users in comparison to *Time Division Multiple Access* (TDMA) and *Time Division Duplex* (TDD) schemes. One of the key strengths is that each transmitter can use a number of codes in order to send multiple information together. Each transmitter has also its own code which distinguishes it out of other that might be using the same frequency in the same geographical area [8].

In the uplink, all signals should arrive on equal signal power at the BS in order for the near-far-effect to be avoided. WCDMA uses power control to cope with this problem and more specifically it adjusts the strength of the transmitted signal of each UE so that it reaches the nearest BS at the same strength as all the other users regardless of the UEs' distance from the base station. The avoidance of receiving excessively strong or weak signals avoids the limitation to the system's efficiency [6].

2.1.2 Uplink Physical Channels

In WCDMA, transport channels are mapped to different physical channels in order to be sent over the air. The physical channels will play a major role on the current study and thus brief explanation will be given. For more information the reader is referred to the book [6].

The two physical channels that are used in this study are

Dedicated Physical Data Channel (DPDCH) DPDCH carries payload data and higher layer signalling. There can be no or several DPDCHs for each radio link.

Dedicated Physical Control Channel (DPCCH) DPCCH carries control information like:

- Pilot bits: used to support channel estimation at the receiver.
- TFCI: Transport Format Combination Indicator.
- FBI: Feedback Information, needed when transmit diversity is active.
- TPC: Transmit Power Control, used to control the transmitted power.

In our uplink simulation we assume that we have four physical channels: one DPDCH, one DPCCH and two high speed channels that have four times more power than the aforementioned dedicated physical channels. Furthermore, power control is not implemented as it is not needed for only one user.

Uplink Radio Frame Structure

The basic frame construction for the uplink is one Super Frame comprising 72 frames. One frame consists of 15 slots and one slot contains 2560 chips, where chip is the unit data after spreading [6].

At the WCDMA uplink, DPDCH and DPCCH are code multiplexed and modulated on the I- and Q- channel, respectively. The uplink frame structure that used in WCDMA is illustrated in Figure 2.1.

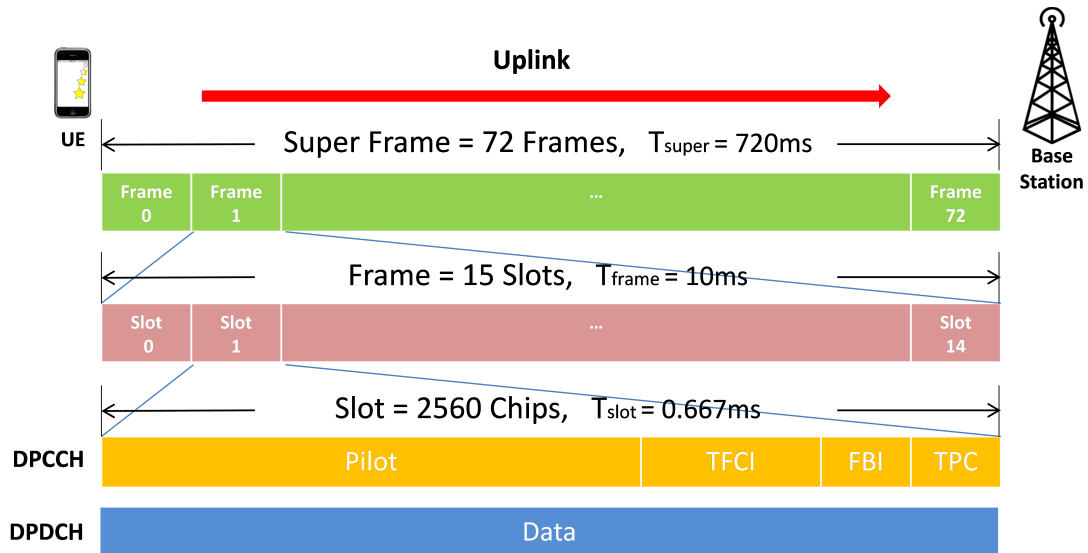


Figure 2.1: The uplink dedicated channel frame structure used in WCDMA

2.1.3 Main Parameters of WCDMA Uplink

The WCDMA uplink main parameters are presented in Table 2.1 [6].

Table 2.1: WCDMA uplink main parameters

WCDMA uplink main parameters	
Channel Bandwidth	5 MHz
Duplex Mode	FDD/TDD
Spread Spectrum Technique	DSSS
Chip Rate	3.84 Mcps
Frame Length	10 ms (38400 chips)
Slot Length	0.6667 ms (2560 chips/slot)
Spreading Modulation	Dual-Channel QPSK with complex spreading circuit
Data Modulation	2 BPSK channels
Channel Coding	Convolutional code, Turbo code, and no coding
Spreading Factors	4-256 for DPDCH, 256 DPCCH

2.2 WCDMA Uplink Simulator

This section describes the WCDMA uplink simulator which we implemented in Matlab. The simulator was implemented in order to evaluate the uplink performance. Data is transmitted frame by frame over a time-varying multipath channel. Turbo coding, spreading and scrambling, oversampling and pulse shaping are carried out before the signal is sent out to the channel. Before transmitting through the channel, there is the PA which is responsible for the signal power amplification. In reality, together with the amplification the PA introduces the AM/AM and AM/PM distortions [2]. Nevertheless, since this study is focused only on the AM/PM phenomenon, the PA is treated like a component which introduces only the phase distortion. Furthermore, *Additive White Gaussian Noise* (AWGN) is added at the end of the multipath channel modelling. At the receiver side the G-Rake is implemented in order to be able to distinguish the multipath components, which results in a better reception [9].

The block diagram of our simulator is illustrated in Figure 2.2.

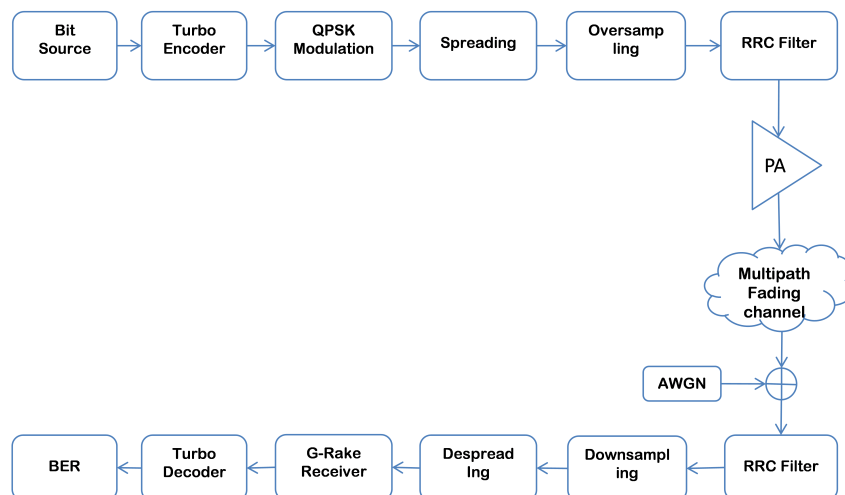


Figure 2.2: A block diagram of the locally developed WCDMA uplink simulator

2.2.1 Digital Modulation

There are three major classes of digital modulation techniques used to map bits into symbols. The information bit stream is encoded in either amplitude (ASK), frequency (FSK) or phase (PSK) of the transmitted signal. By using k bits per symbol, the bit rate turns to symbol rate and thus the system can provide the user higher transmitting speeds with higher values of k [8].

WCDMA uses two orders of PSK modulation. Order 1 where 1 bit per symbol is transmitted is called BPSK and order 2 where 2 bits are transmitted per symbol is named QPSK. WCDMA can transmit even faster by using QAM. In the 3GPP standard there

can even be 8 bits per symbol resulting in 256-QAM. Nevertheless, such high schemes require very good channel conditions. In reality, such conditions can vary from occurring rarely to almost never, especially if the user is far away from the BS. In this study QPSK is chosen for the simulation. The QPSK signal constellation is displayed in Figure 2.3. For more information about modulation techniques, the reader is referred to the book [10].

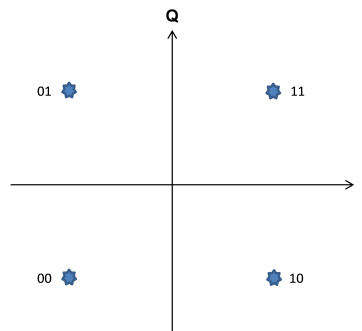


Figure 2.3: QPSK signal constellation with Gray coding.

2.2.2 Channel Coding

Channel coding (error correction coding) is a way of mitigating bit errors that are produced by the channel. Extra bits are added to the transmitted signal in order for the receiver to be able to detect and correct some of the erroneous bits. Two coding schemes are used in UTRAN: convolutional codes and turbo codes. Convolutional codes are better used for low data rate and turbo codes are used for high data rate scenarios [8]. For the current study the turbo codes are used as our error correction scheme.

Turbo Codes

The turbo encoder of the Matlab Communication toolbox is used in order to generate the redundant bits as well as the interleaver needed. With turbo codes, a better *Bit Error Rate* (BER) performance can be achieved than without channel coding [11], and that can be seen by comparing between the BER to the raw BER which is calculated before turbo decoding.

2.2.3 WCDMA Codes

WCDMA coding operation consists of spreading and scrambling. Spreading is used to distinguish multiple data channels from each transmitter. Scrambling on the other hand is used to distinguish multiple transmitters in WCDMA.

Spreading Codes

Spreading codes are orthogonal codes that are used for channelization. Spreading codes define how many chips are used to spread a single information bit and determine the end chip rate. The chip rate in WCDMA uplink is 3.84 mega quarter-chips per second (Mqcps), which means one frame of 10 ms will spread into 38400 chips. Spreading helps preserving the orthogonality amongst different physical channels of an uplink user such that different data channels coming from each UE to each cell can be separated. In principle, each physical channel corresponds to a unique spreading code, used to separate transmissions from different users [12]. With different spreading codes, we can have multiple channels sent from the same transmitter.

In WCDMA uplink, *Orthogonal Variable Spreading Factor* (OVSF) codes are used for spreading. The key function of OVSF codes is the orthogonality between different physical channels which happens by multiplying the data stream with unique spreading codes. The generation of OVSF codes can be seen in Figure 2.4 [12].

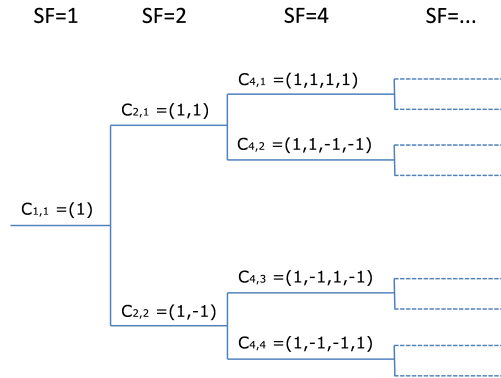


Figure 2.4: OVSF codes tree

The code in each tree level defines the spreading code of spreading factor length(SF). All the OVSF codes for the same level have zero cross correlation. Any two codes of different levels are orthogonal to each other as long as one of them is not the parent of the other [13].

Spreading Factor

The length of spreading codes is referred to as spreading factor. As the quantity of spreading codes is also limited by Spreading Factor (SF), the maximum different channels which can be sent by the same transmitter is thus limited by SF.

The spreading factor of DPCCH is 256. and the spreading factor of DPDCH varies between 4 and 256 in the WCDMA uplink.

Spreading working process

Spreading works by multiplying every data bit with the spreading sequence, and generates chip rate $R \times SF$ chips as a consequence. In the receiver, the descrambled spread signal is obtained by multiplying every SF-length block of chips with the spreading code, and then for the same length the chips are summed to reconstruct the original transmitted bit.

An example of the spreading and despreading functionality would be: assuming C_1 is the spreading code for channel 1 (CH_1) for UE, C_2 for channel 2 (CH_2) and C_3 for channel 3 (CH_3) for the same UE, where C_1 , C_2 and C_3 are orthogonal to each other. Then the transmitted signal becomes $CH_1 \times C_1 + CH_2 \times C_2 + CH_3 \times C_3$. In the despreading part, C_1 is used to despread CH_1 and in the same way, C_2 , C_3 are used for despreading CH_2 , CH_3 , respectively, to get their own signals.

The following equations instruct the process of the CH_1 despreading:

$$\begin{aligned}
 & (CH_1 \times C_1 + CH_2 \times C_2 + CH_3 \times C_3) \times C_1 \\
 &= CH_1 \times (C_1 \times C_1) + CH_2 \times (C_2 \times C_1) + CH_3 \times (C_3 \times C_1) \\
 &= CH_1 \times 1 + CH_2 \times 0 + CH_3 \times 0 \\
 &= CH_1.
 \end{aligned} \tag{2.1}$$

Scrambling Codes

Scrambling codes are used to distinguish multiple WCDMA transmitters, and those sequences are non-orthogonal. In WCDMA, every user is assigned a unique code, and the receiver multiplies the received signal with the known corresponding scrambling codes to recover to the original signal.

As the scrambling codes are non-orthogonal sequences, therefore in our simulator we can just generate some random flipping bits as our scrambling code. Descrambling is similar to despreading, the received signal is just multiplied with the scrambling codes to get the original signal. Figure 2.5 and 2.6 illustrate how the WCDMA uplink spreading scrambling and despreading descrambling is implemented.

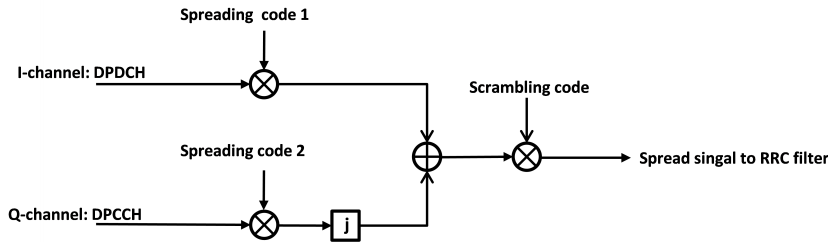


Figure 2.5: WCDMA uplink spreading and scrambling functions

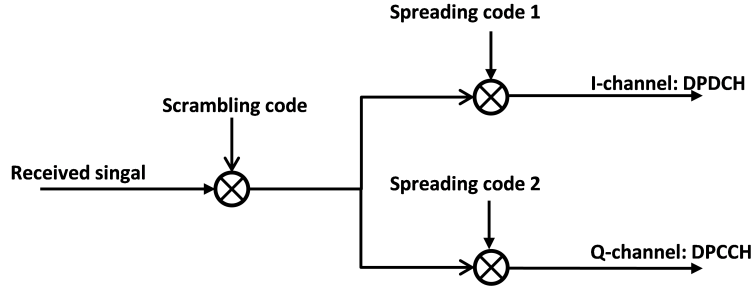


Figure 2.6: WCDMA uplink despreading and descrambling functions

2.2.4 Pulse Shaping and Matched Filter

Pulse shaping can minimize the *Inter Symbol Interference* (ISI) during pulse transmission. A *Raised Cosine* (RC) filter is one of the widely used pulse shaping filters. The implementation of an RC filter is split into one *Root Raised Cosine* (RRC) filter at transmitter and another matched RRC filter at the receiver. The cascade of two RRC filters is equivalent to one RC filter. According to the Nyquist theorem, before passing our signal in chip level through the first RRC filter, we need to oversample the signal into samples (quarter-chips level) to avoid aliasing [14]. After passing through the second RRC filter, we do downsampling to recover the received signal into the chip level.

The WCDMA, according to 3GPP standardisation, has a channel bandwidth of 5 MHz. The roll-off factor of the RRC filter in WCDMA is specified to be 0.22, and it is a measure of the excess bandwidth of the filter. The chip rate of WCDMA is 3.84 Mcps. Thus, the occupied bandwidth after the RC filter is $1.22 \times 3.84 = 4.68$ MHz. If oversampled by a factor of 4, the rate is $4.68 \times 4 = 15.36$ Mcps.

2.2.5 Multipath Propagation

Objects that exist in the environment cause multiple reflections, refractions, diffractions and attenuations on the signal. The result of all of these phenomena is the so-called multipath propagation. Due to the different distances to the various interacting objects the energy is arriving to the receiver with different delays. The power for different paths is also varying due to the fact that each path is subjected to different degrees of attenuation [6]. In our study, we assume a Rayleigh channel model which is called Pedestrian-A at 3km/h (PA3) [15]. To deal with this kind of channel, we use G-Rake receiver to combine the energy. Detailed explanation regarding G-Rake receiver can be found in later sections.

Figure 2.7 illustrates the multipath propagation phenomenon and Figure 2.8 shows the PA3 Rayleigh fading channel.

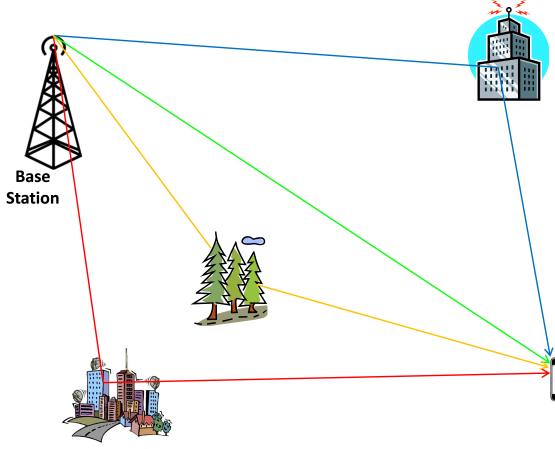


Figure 2.7: Multipath propagation from base station to user equipment

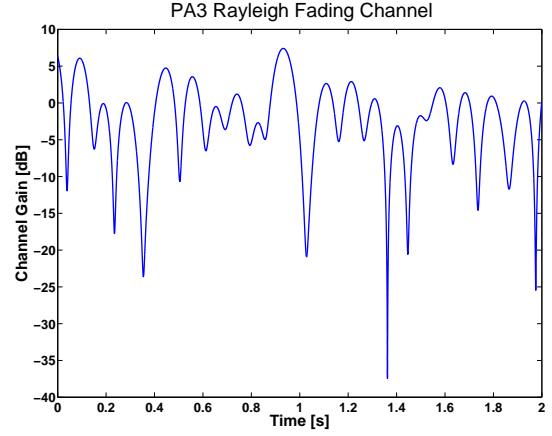


Figure 2.8: One realisation of a Rayleigh fading channel caused by multipath propagation (PA3)

2.2.6 Channel Estimation

Channel estimation is needed for the RAKE and G-Rake receivers when calculating the weights of each path. The sub-receiver on each path is called finger in this receiver. In our study, we assume close to perfect channel estimation where the *Signal to Noise Ratio* (SNR) is very high and so we can also assume zero noise.

In this report, boldface is used to denote vector notation which contains several values due to multipath. Assuming we have n paths, the vector $\mathbf{y}_n = [y_1 y_2 \cdots y_n]$ means received symbols on path 1, 2, \cdots n respectively. Given the received signal after demodulation

$$\mathbf{y}_n = \mathbf{h}_n s + \mathbf{u}_n, \quad (2.2)$$

we can get a channel estimate $\hat{\mathbf{h}}_n$ by dividing the received signal by the transmitted signal

$$\hat{\mathbf{h}}_n = \frac{\mathbf{y}_n}{s} = \mathbf{h}_n + \frac{\mathbf{u}_n}{s}, \quad (2.3)$$

where \mathbf{h}_n is the true channel, s is the pilot symbols, \mathbf{u}_n is the noise which will be explained in the next sections. n defines the tap.

2.2.7 Receiver Diversity

Due to high attenuation that are produced by fading deeps, fading channels are introducing a large number of errors to digital communication systems. The probability that a fading deep will appear can be decreased considerable by the fact that the information that arrives on the receiver at different delays due to the attenuation is faded

independently. Therefore, not all the replicas of the multipath will be highly attenuated decreasing the probability of error and thus gaining receiver diversity. This happens by extracting the information through those independently attenuated paths and then by adding them coherently. One such method is *Maximum Ratio Combining* (MRC) for which detailed information can be found in [10]. RAKE and G-Rake are receivers that use MRC to maximise SNR. Both of them will be explained in detail on the following sections.

RAKE Receiver

The RAKE receiver extracts diversity using the multiple paths of a fading channel. RAKE fingers which contain correlators are connected to the dominant delay taps in order to capture the multiple replicas of the transmitted signal [16].

The RAKE receiver is called like that due to its actual functionality that bears resemblance to a garden rake where each finger picks a dominant tap. Despite the fact that an individual signal might prove really weak to produce a correct result, the coherent combination of many weak signals can provide more than enough energy to receive the combined signal correctly.

The multipath channel has a typical delay profile that extends from 1 to 2 μs in urban and suburban areas and sometimes grows to more than 20 μs for hilly areas. A WCDMA chip with a chip rate of 3.8 Mcps has a time duration of 0.26 μs . This makes it possible that if between the multipath components there is a span of at least that duration then the WCDMA receiver can distinguish and separate those multipath components and combine them coherently to gain the desired multipath diversity [6]. Figure 2.9 shows the multipath components combination of the RAKE receiver.

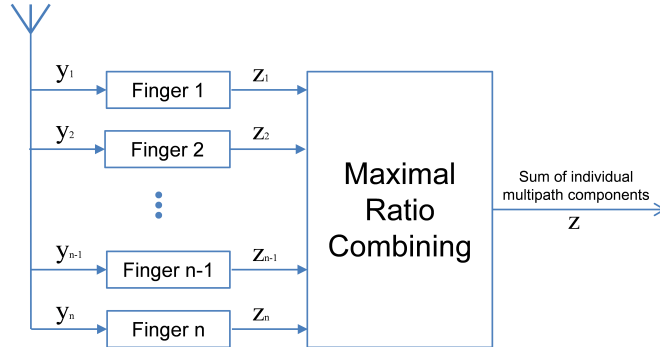


Figure 2.9: RAKE receiver

Using a vector notation then, received signals on the receiver with one antenna can be seen in Eq. (2.4)

$$\mathbf{y}_n(m) = \mathbf{h}_n(m)s(m) + \mathbf{u}_n(m), \quad (2.4)$$

where n defines the tap or the finger associated on these tap, m is the current symbol,

$\mathbf{y}_n(m)$ is the received symbol, $\mathbf{h}_n(m)$ is the channel coefficients, $s(m)$ is the transmitted symbol and $\mathbf{u}_n(m)$ is the noise.

Then when the fingers correlators are applied it will result in the following finger output

$$\begin{aligned} z_n(m) &= \mathbf{w}_n^H(m)\mathbf{y}_n(m) \\ &= \mathbf{w}_n^H(m)\mathbf{h}_n(m)s(m) + \mathbf{w}_n^H(m)\mathbf{u}_n(m). \end{aligned} \quad (2.5)$$

These finger outputs can be then maximal ratio combined to produce our estimated symbol. More detailed explanation about the RAKE receiver can be found in Appendix A.

G-Rake Receiver

The noise \mathbf{u}_n is modelled including the self-interference that comes from intra-symbol interference when a symbol s_n interferes with itself from another path due to multipath, the self-interference emerging from inter-symbol interference that happens when the symbol s_n interferes with past and future symbols s_k where ($k \neq n$) and the interference coming from other sources which could be the multiplexing of users or thermal noise [9]. In the RAKE receiver the multipath components are distinguished and separated but the coloured noise is not yet compensated as RAKE is designed for white noise. On the other hand, the G-Rake receiver achieves interference suppression by whitening the noise with the help of the correlation across the fingers and then adapting the combining weights on the fingers. The performance of the G-Rake receiver can be improved by increasing the number of fingers beyond the number of multipath components [17]. Finger placement is another factor that can affect the performance of the G-Rake receiver. We will not emphasise it here rather than give the G-Rake receiver expressions.

For an estimated impairment covariance matrix equal to

$$\hat{\mathbf{R}}_{\mathbf{u}} = E[\mathbf{u}_n\mathbf{u}_n^H], \quad (2.6)$$

the G-Rake finger combining weights \mathbf{w}_n are obtained by multiplying the channel coefficients with the inverse covariance matrix

$$\mathbf{w}_n = \hat{\mathbf{R}}_{\mathbf{u}}^{-1}\hat{\mathbf{h}}_n. \quad (2.7)$$

It should be observed that in the case of the RAKE receiver it is easy to understand that the covariance matrix $\mathbf{R}_{\mathbf{u}}$ becomes the identity matrix \mathbf{I} where $\mathbf{R}_{\mathbf{u}} = \sigma_u^2\mathbf{I}$. More information about the G-Rake receiver can be found in article [17].

2.3 Power Amplifier Model

Amplifiers produce distortion which is introduced to the transmitted signal. This distortion can affect both the amplitude as well as the phase of the transmitted signal. The design of power amplifiers depends much on the variation of the signal envelope. For these variations it is useful to have a measure of description. *Peak-to-average Power Ratio* (PAPR) is such a measure and it defines the ratio between the maximum value of

the square of the signal divided by the average of its squared value [18]. In the following sections the distortion will be characterised.

The output of an ideal amplifier would be the exact copy of the input signal multiplied by a scaling factor. That would be translated in the following equation

$$V_{out}(t) = GV_{in}(t), \quad (2.8)$$

where V_{in} is the input voltage, V_{out} is the output voltage and G is the scaling factor, or voltage gain, that the amplifier should produce.

In reality the amplifier is not perfect. The output of the PA cannot linearly increase for any input value. There is a voltage region which is called PA saturation region where an increase in input power does not produce an equal increase in the output power and therefore the PA saturates [19]. The scaling factor therefore becomes dependent on the input voltage and that distortion is named AM/AM and it can be modelled by in the following equation

$$V_{out}(t) = G(V_{in}(t))V_{in}(t). \quad (2.9)$$

Non-linearity distortions do not only apply to the amplitude but also to the phase by the so called AM/PM distortion phenomenon. There the phase of the signal is being shifted by a number of degrees dependent, again, on the input power.

In the literature [2] there are various models that describe the non-linear functionality of a power amplifier. In order to measure these distortions methods like the Two-Tone test is used that the reader can find in [20], [21]. In this study the Saleh model and a polynomial model are considered and measurements previously done from Ericsson provide us with the values for the models.

2.3.1 Saleh Model

In the Saleh model, the non-linear functionality of the amplifier is defined using two parameters. One parameter defines the amplitude characteristics and the other defines the phase distortion. Each parameter contains two basic variables that can be modified in order to characterise these distortions [2].

The AM/AM is described by the parameter

$$G(V_{in}) = \frac{\alpha_a V_{in}}{1 + \beta_a V_{in}^2}, \quad (2.10)$$

where α_a and β_a are the variables that characterise the amplitude gain of an input power V_{in} .

The AM/PM is described by the parameter

$$\Phi(V_{in}) = \frac{\alpha_\phi V_{in}^2}{1 + \beta_\phi V_{in}^2}, \quad (2.11)$$

where α_ϕ and β_ϕ are the variables that characterise the phase shift in radians when an input voltage V_{in} is applied to the amplifier.

From a signal point of view, when a signal $\tilde{x}(t)$ is applied to the amplifier with a variable voltage $V_{in}(t)$ then the output of the amplifier according to the Saleh model is

$$\tilde{y}(t) = G(V_{in})e^{j(\phi(\tilde{x}(t))+\Phi(V_{in}))}, \quad (2.12)$$

where $\phi(\tilde{x}(t))$ is the phase of the input signal.

2.3.2 Polynomial Model

Another way to show the AM/AM and AM/PM characteristics is to apply a polynomial model for both $G(V_{in})$ and $\Phi(V_{in})$ [2].

$$G(V_{in}) = a_0 + a_1A(V_{in}) + a_2A(V_{in})^2 + \dots + a_nA(V_{in})^n \quad (2.13)$$

$$\Phi(V_{in}) = b_0 + b_1A(V_{in}) + b_2A(V_{in})^2 + \dots + b_nA(V_{in})^n \quad (2.14)$$

The coefficients of the polynomial model can be obtained from measurements using the *Least Squares Estimator* (LSE) [22].

3

Distortion Characterisation and Simulation Results

The following chapter covers our simulations as well as the results of them considering the phase distortion introduced by the PA. Firstly, we present the reader with the implementation of the simulation chain while including the most important details that make the system realistic. Then the PA distortion implementation is given, which is a practical approach that complies with the existing in literature models. Lastly, results about important metrics are thoroughly discussed. After the motivation of the system results, it should be clear whether and how much the PA phase distortion affects the system performance.

3.1 Simulator Implementation

For our simulations, we use parameter values that represent WCDMA. These values are shown in Table 2.1. In order for our system to be as much realistic as that its results can be trusted, most of the values needed that are already standardised for WCDMA from 3GPP are used in our system without any changes to them. There are values which in terms of complexity have been altered, though these alterations do not affect the results.

3.1.1 WCDMA Configuration

To configure the WCDMA uplink simulator we kept all the parameter values from the WCDMA standardisation unchanged and varied the power amplifier distortion. Data is transmitted frame by frame according to 3GPP specifications. The number of frames is flexible in this simulator depending on how much data we want to transmit. The number of slots, chips, chip rate and other variables related to WCDMA are fixed in the initialisation.

In order to see the impact of power amplifiers, HS-channels are added asynchronously on top of normal channels. Figure 3.1 shows the discontinuous HS-channel pattern we added on both DPDCH and DPCCH. The vertical axis is the amplitude of signal and the horizontal axis is number of symbols in time domain as slot unit. It should be observed that the amplitude of symbols on HS-channel is twice that of the original physical channels. In the implementations, the transmitted signal on data channel and control channel is the summation of symbols on both HS-channel and normal channel. As explained before, different spreading codes are used here to differ HS-channel data and DPDCH/DPCCH data in the receiver.

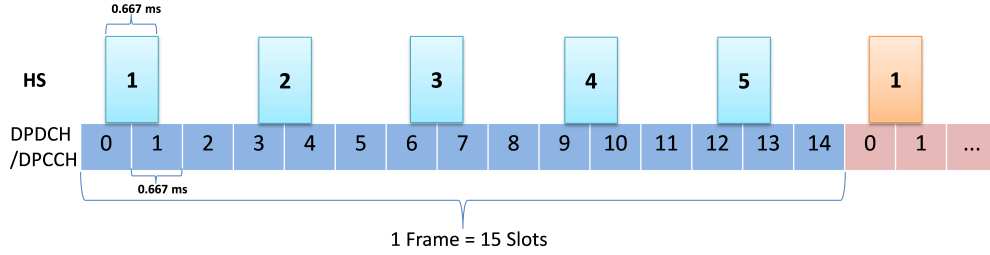


Figure 3.1: High speed channel on top of DPDCH and DPCCH. (The HS has 4 times the power of DPDCH/DPCCH, and it has a specific burst pattern as shown.)

3.1.2 SNR Calculation

For our simulation, each bit transmitted turns into 3 turbo coded bits. Then each turbo coded bit turns into 64 spread chips. Finally each chip turns into 4 quarter-chips or samples. Assuming now that the lowest energy element is a quarter-chip and the energy of a quarter-chip equals to the unity as in $E_{qc} = 1$ then the energy of a bit can be represented as

$$E_b = \frac{1}{R} \cdot OS \cdot SF \cdot E_{qc}, \quad (3.1)$$

where R is the turbo code rate, OS is the oversampling rate, and SF is the length of spreading code.

One important note is that since we are studying uplink where the physical channels are completely independent of each other, then our QPSK stream can easily be translated into two BPSK streams orthogonal to each other. So our basic SNR metric shall be E_b/N_0 for each particular stream.

Then assuming a predefined E_b/N_0 , we calculate the noise variance as follows.

$$SNR = \frac{E_s}{N_0} = \frac{2E_b}{N_0}, \quad (3.2)$$

then

$$2E_b/N_0 = \frac{2 \frac{1}{R} \cdot OS \cdot SF \cdot E_{qc}}{N_0}, \quad (3.3)$$

therefore

$$\begin{aligned}
 N_0 &= \frac{2^{\frac{1}{R}} \cdot OS \cdot SF \cdot E_{qc}}{2E_b/N_0} \\
 &= \frac{\frac{1}{R} \cdot OS \cdot SF}{E_b/N_0}.
 \end{aligned} \tag{3.4}$$

Figure 3.2 shows how we define the SNR in our simulation directly: we fix the signal power and make the noise power spectral density vary to alter the SNR. For example, as the signal power is always fixed to 1, to obtain 6 dB, we need to make the noise power percentage into 0.25 which is the corresponding 25% in the vertical axis. According to the Eq. 3.4, we implement the variation of N_0 from different values of E_b/N_0 .

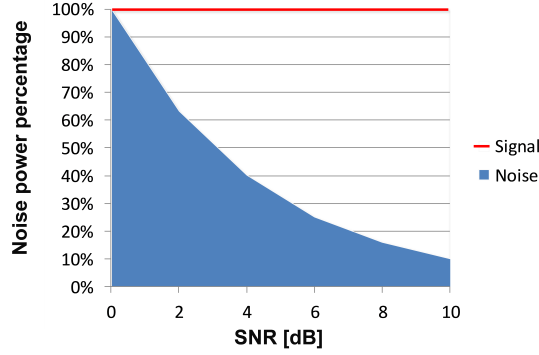


Figure 3.2: SNR definition of the simulator. The red is signal power level which is always fixed to 100% and the blue is noise power percentage which changes according to different SNR in dB compared with unity signal power.

3.1.3 Turbo Coder and Modulation

We use the Matlab communication toolbox to implement the turbo encoder and decoder in our simulator, where 1/3 is the selected turbo code rate. The input bits is 196 and the output of turbo encoder is 600 bits per frame. The pure code rate is $\frac{196}{600}$ but some extra parity bits are added by the turbo encoder and those ones fix the rate at the desired value. For QPSK modulation the symbols are Gray coded.

3.1.4 Rayleigh Fading and Multipath Channel Generation

Two independent Gaussian random variables, one for the real part and one for the imaginary, can be summed into a complex Gaussian random variable. By shaping the random signal in the frequency domain with the Doppler spectrum we get Doppler fading in the frequency domain. The time domain Doppler fading can be easily acquired by using the inverse Fourier transform.

Following the aforementioned procedure, a flat fading tap can be created. For a Multipath Rayleigh channel a number equal to the desired taps must be created and then

added at their respectful delays to finally produce the fading channel [16]. The detailed tap delays of Pedestrian-A 3 km/h used in our simulation can be seen in Figure 3.3.

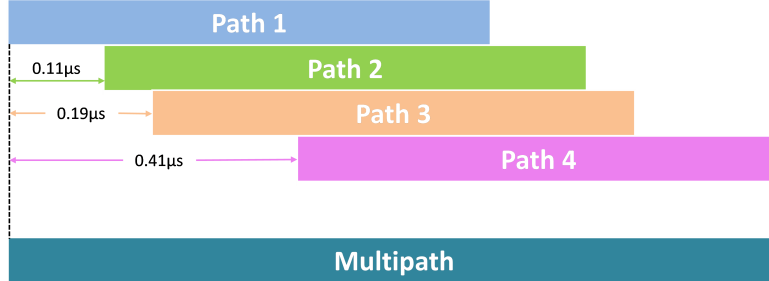


Figure 3.3: Multipath and tap delays at Pedestrian-A 3 km/h. Each tap comes at a specific delay. The summation provides the multipath signal.

The channel model that is used for our simulations is a 4-tap Rayleigh fading multipath channel with delays of 68, 70, 71, 74 quarter-chips. In time these values translate approximately into $0.065\mu s$, $0.175\mu s$, $0.255\mu s$, $0.475\mu s$, respectively. The tap power normalised to the first dominant tap are 0 dB, -9.7 dB, -19.2 dB, -22.8 dB [15]. With these numbers we created our multipath Rayleigh fading channel, and an example of that can be seen in Figure 3.4.

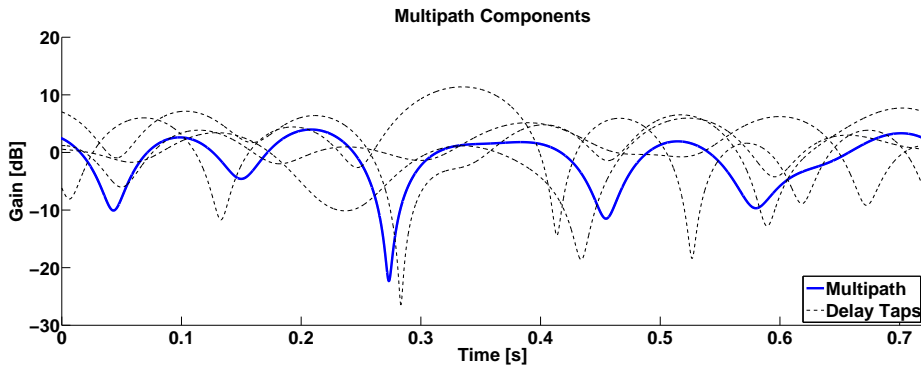


Figure 3.4: Multipath and each path Rayleigh fading channel. This is one realisation of the taps and the summation(multipath) for a duration of one super frame.

3.1.5 Spreading

OVSF codes are used as spreading codes in WCDMA. We use the Matlab communication toolbox to generate the OVSF codes tree and then select the indexes of the desired spreading codes. The spreading factor for DPDCH for a real system can vary from 4 to 256. The length of that spreading code depends on the user data rate, which after spreading guarantees that the output always ends up with a chip rate of 3.84 Mcps. The SF for DPCCH is fixed to 256 but the chip rate has to be the same as DPDCH.

Therefore, the shorter SF sequence will be transmitted at a higher information rate than the longer SF sequence.

In order to simplify our system, we just use SF=64 for both DPDCH and DPCCH in our simulation which result in reducing the complexity of the implementation in Matlab. Nevertheless, this change does not affect the results in our system. To understand the spreading and the despreading process more clearly, Figure 3.5 and 3.6 are showing explicitly how data is spread in the transmitter and despread to recover the original data in the receiver.

In Figure 3.5 two bits of data (red) is XOR with the spreading code (blue) that results into the transmitted signal (green).

$$\text{Spread Signal} = \text{Data} \times \text{Spreading Code} \quad (3.5)$$

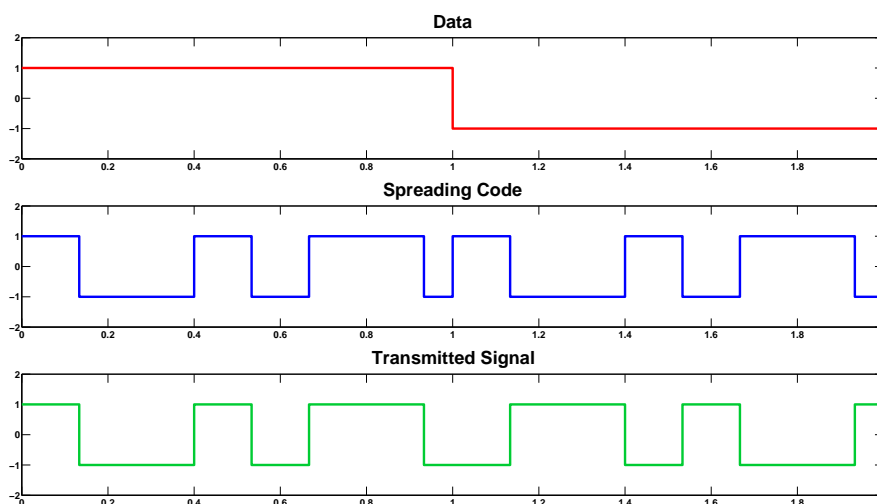


Figure 3.5: Spreading process in waveform. Red is two bits of data that XORs the spreading code(blue) and result in the transmitted signal(green).

In Figure 3.6 the despread data (red) is the result of the XOR of the received signal (green) and the same spreading code (blue) as used in the transmitter (Figure 3.5).

$$\text{Data} = \text{Spread Signal} \times \text{Spreading Code} \quad (3.6)$$

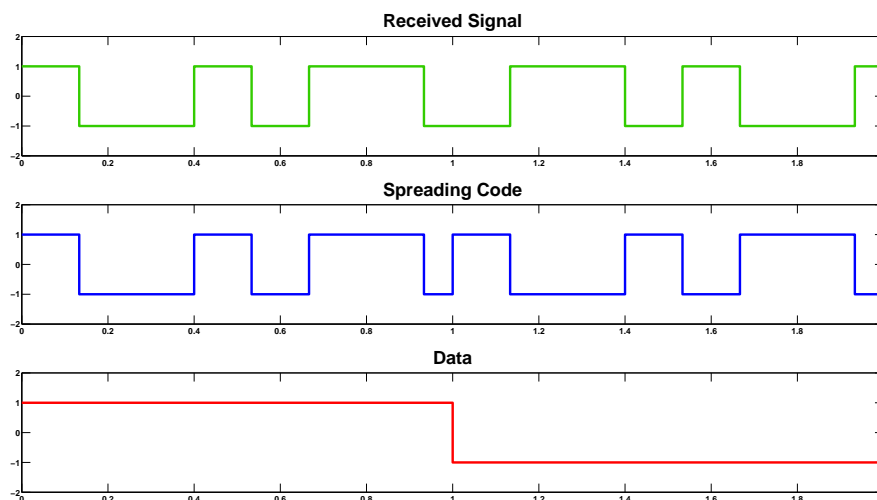


Figure 3.6: Despreading process in waveform. The received signal (green) is XORed by the spreading code (blue) which results in our data (red).

3.1.6 Channel Estimation

For the channel estimator we follow the exact procedure we explained in Chapter 2.2.6. We assume a perfect channel where there is no noise. From Eq. 2.2 for a very high SNR \mathbf{u}_n is assumed to be very small and thus we can neglect it. So for a received signal $\mathbf{y}_n = \mathbf{h}_n s$ to acquire \mathbf{h}_n , we just divide with the transmitted signal s which plays the role of the pilots.

In real systems the pilots have high energy and are sent as regularly as the channel varies in time. For our simulator the channel can be considered static for a time interval of one slot. In Figure 3.7 the estimated channel is calculated and compared with the true channel. A reasonable approximation is achieved.

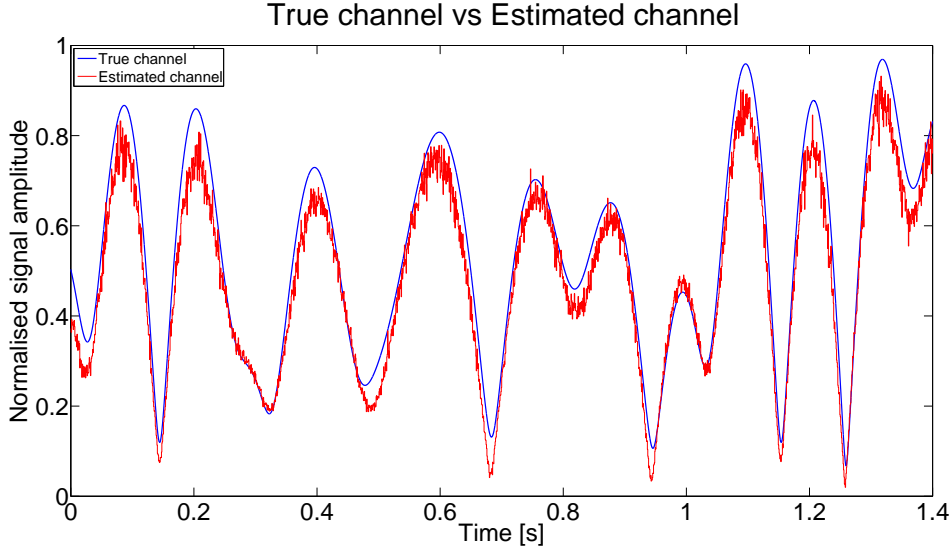


Figure 3.7: True channel and estimated channel comparison. One realisation of the estimated channel coefficients for two super frames. The comparison with the true channel gives a reasonable fit.

3.1.7 G-Rake Receiver

In the principle of a RAKE receiver the system should be able to distinguish the various fading taps both in terms of delay and gain. For our link simulator we have got a perfect channel estimator from which we get to know the exact delays and gains of the multipath taps. Thus, with that information we can extract our fingers for the receiver.

The differences between a RAKE receiver and a G-Rake receiver come in the noise impairment covariance $\hat{\mathbf{R}}_{\mathbf{u}} = \mathbb{E}[\mathbf{u}_n \mathbf{u}_n^H]$ in order to whiten the coloured noise that reality provides, and the additional fingers that can be added in the system to improve the performance [9].

The impairment covariance is calculated for every slot as the channel remains static for that time duration. Then the channel estimates are multiplied with the inverse covariance in order to acquire the finger weights (see Eq. (2.7)).

The resolution we have for the finger placement for the G-Rake receiver comes of course at a quarter-chip level. The G-Rake shall put a finger on all the multipath taps. Defining that our simulation starts from chip 0 then the fingers are placed at quarter-chip 0, 2, 3 and 6 as the delays in between them are shown in Figure 3.3 where the first quarter-chip is the start of the first tap and then the other quarter-chips take respectively the beginnings of the next taps. The additional fingers placement have been chosen to cover every quarter-chip in between and one before and after the existing ones as shown in Figure 3.8.

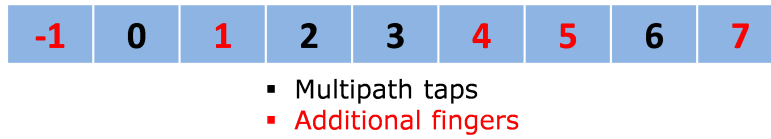


Figure 3.8: G-Rake receiver finger placement. A finger is assigned for both red and black place.

Furthermore, our despread estimated physical channel is multiplied with the conjugate of the finger weights in order to acquire the raw symbols for each sent physical channel. Those raw symbols are then forwarded in the turbo decoder.

3.2 PA Distortion Characterisation

This section will describe the Saleh model and a polynomial model configurations that we used and their theoretical effects together with their actual effects on our system.

3.2.1 Saleh Model

To begin the characterisation of the distortion of an amplifier at a UE we started using the Saleh model. As mentioned previously in Chapter 2 the Saleh model can provide us with AM/AM and AM/PM conversion just by altering two variables for each conversion. For an amplifier that would be realistic in terms of phase distortion and amplification values were to be found that would produce distortion and amplification that could match a real UE. A typical PA at the UE usually provides a gain of 35 dB [14] and provides no more than 8 degrees of phase distortion. For a realistic signal which has incoming voltage from 0 to 0.4 volts for our Saleh model, the resulting behaviour can be seen in Figure 3.9 with the variable settings in Table 3.1.

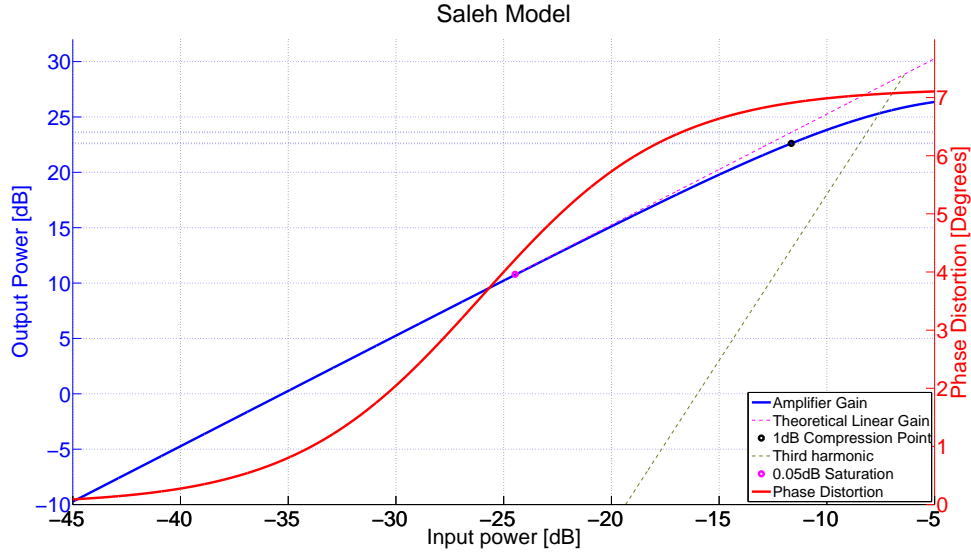


Figure 3.9: Saleh model AM/AM and AM/PM. On the left side lies the output power in dB shown by the blue curve in comparison with input power. The red curve shows the phase distortion which applies for a specific input power.

Table 3.1: Saleh model variable values used in our simulator

Parameter	Variable	Value
Amplitude	α_a	58
	β_a	1.8
Phase	α_ϕ	50
	β_ϕ	400

The signal that enters the PA is on a quarter-chip level thus the E_{qchip} has now to be normalised on new levels so that the energy is appropriate for the formulas in Chapter 3.1.2.

After applying such a signal to the amplifier model the reader can see the percentage of the signal in comparison with the respective phase distortion that the Saleh model provides in Figure 3.10.

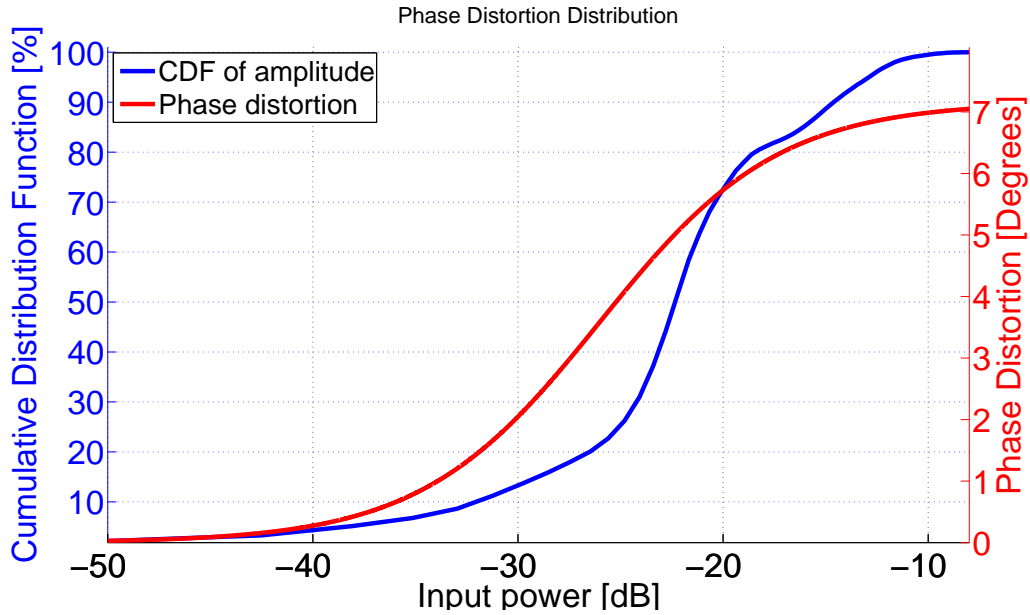


Figure 3.10: Saleh model phase distortion distribution. The blue curve is the CDF of input signal's amplitude. The red curve explains the corresponding phase distortion of that input power.

To read the upper figure, for example: look at -20dB on X-axis, there are around (100-70=30 %) samples which have input power higher than -20dB will have around 5.5 degree phase shift. We can read from the *Cumulative Distribution Function* (CDF) curve that most(70 %) of our input signal will have the phase shift of 2.2 degree.

In Figure 3.10 it can be clearly seen that the signal is affected by various phase distortions according to its amplitudes and thus its constellation is expected to be rotated. This rotation can be seen in Figure 3.11 where the quarter-chips of a single frame are being affected by the PA rotation before they are sent to the channel.

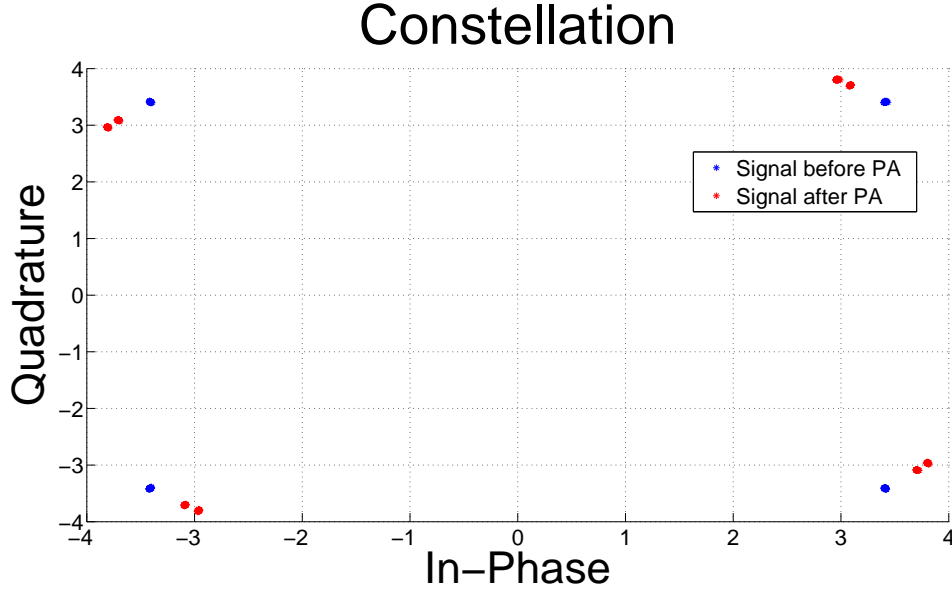


Figure 3.11: Saleh model constellation rotation after the added PA phase distortion

Figure 3.11 shows the constellation of the signal before PA (blue dot) and signal after PA (red dot). Please note that, the input signal for Figure 3.10 is after oversampling, scrambling and spreading, so from there you can see continuous phase distortion for continuous input signal. In the upper figure, the phase shift is gotten from signal after down-sampling, descrambling and despreading. The reason why there are two dots suffered different phase shift from PA is that we have different power level for DPDCH/DPCCH and high speed(HS)-channel whose amplitude is double of the normal channel in our implementation (refer to section 3.1.1 for details). As we know the phase shift depends on the amplitude of input signal and there are basically two main level of signal amplitude (0.13 volts for DPDCH/DPCCH and 0.4 volts for HS-channel) after normalization, so basically there should be two main kinds of phase shift on the constellation.

It is obvious from Figure 3.11 that the phase distortion behaves in constant way. This means that the whole constellation seems to be having two constant values as phase distortion which will be corrected by the channel estimator. The signal then is not expected to change its behaviour on the decoder due to the current PA distortion.

3.2.2 Polynomial Model

In order to make our results more realistic, it was decided to use the polynomial model to confirm the modelling of Saleh. This time a memoryless polynomial was to be applied based on Ericsson internal measurements of a typical UE PA for WCDMA/LTE and the resulting phase distortion was to be introduced to the transmitted signal. The input signal's amplitude was again normalized between 0 to 0.4 volts to comply with voltages that are used on real WCDMA systems and that resulted in the following AM/AM and

AM/PM conversions that are shown in Figure 3.12.

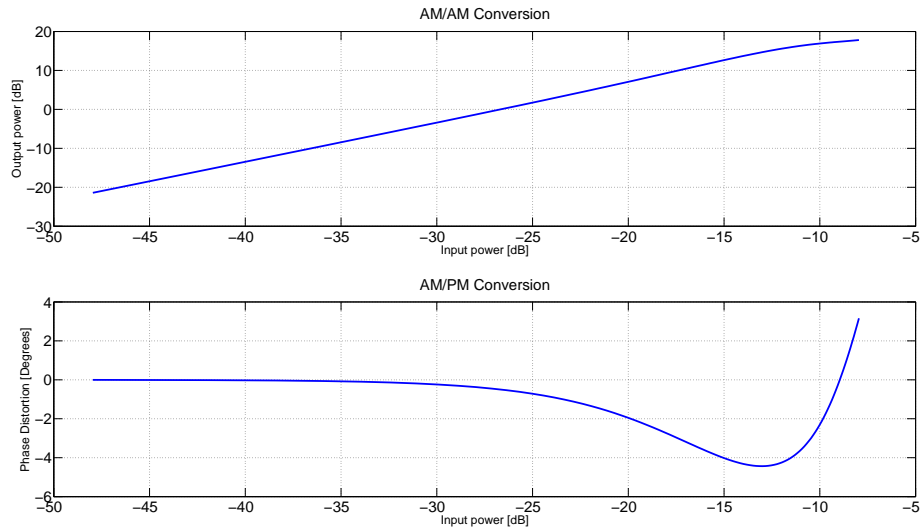


Figure 3.12: Polynomial model AM/AM and AM/PM. Typical characteristics of a UE power amplifier. The PA is quite linear for most of the input values.

One can see the high linearity of such a typical PA for UE and that the range of degrees varies from -4 to 4 degrees considering again the input predefined amplitudes. The actual effects of the model can be seen on Figure 3.13 where the phase distortion is distributed across the amplitudes of the oversampled signal.

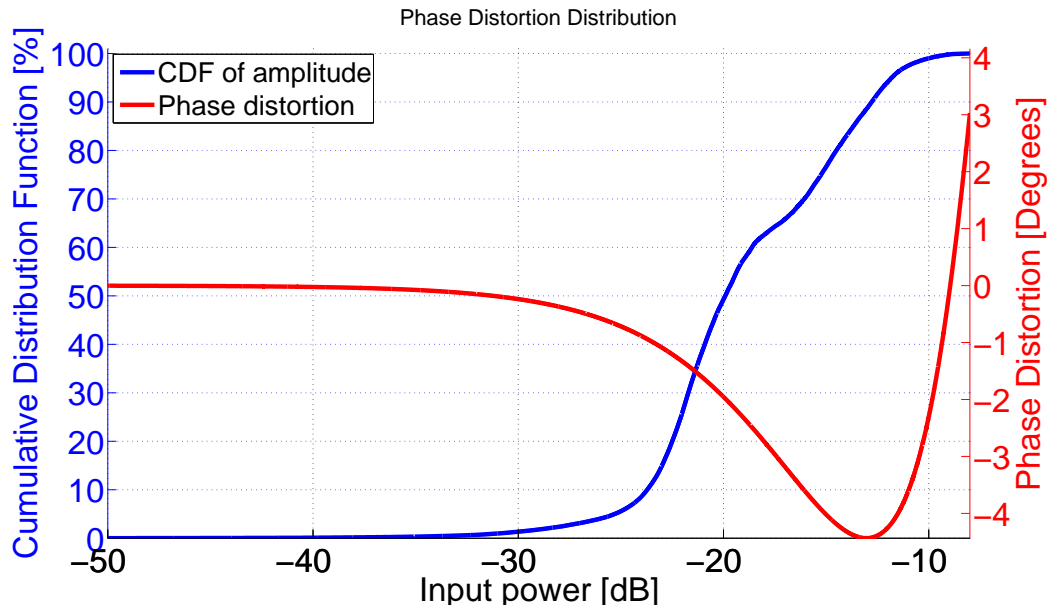


Figure 3.13: Polynomial model phase distortion distribution. The blue curve is the CDF of input signal's amplitude. The red curve explains the corresponding phase distortion of that input power.

The observation of the phase distortion of the applied polynomial is that the signal acquires negative angles from the PA, which nevertheless translates into a constellation rotation. That constellation rotation can be seen in Figure 3.14 where the more realistic polynomial model rotates the signal even less than the Saleh model. Such a behaviour is going to be even less detrimental for the signal and therefore the BER performance is not expected to be affected by any considerable values.

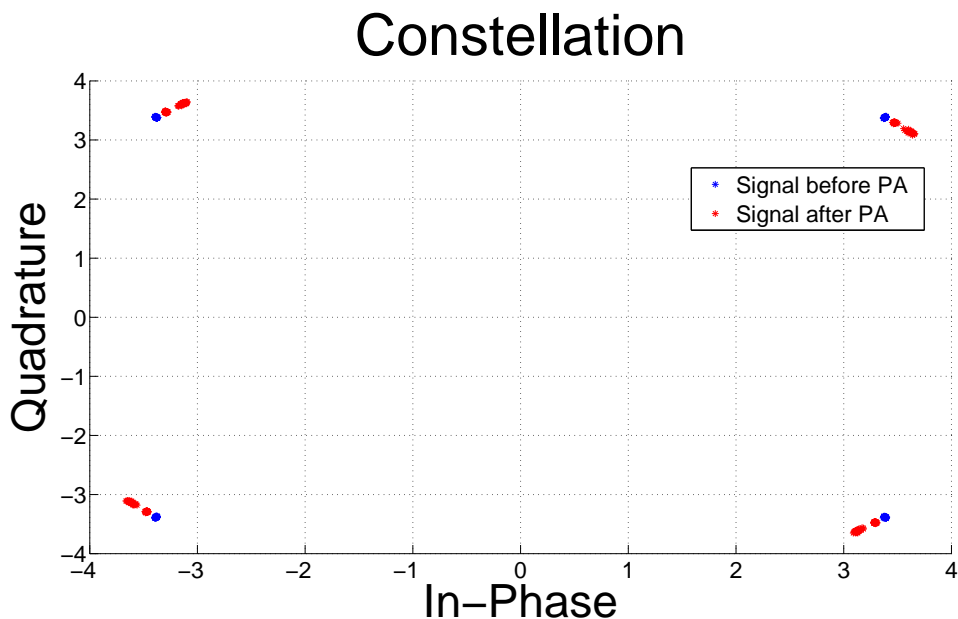


Figure 3.14: Polynomial model constellation rotation after the added PA phase distortion

3.3 Simulation Results

The following section will provide with the system performance of both tested PA models. That will include the bit error probability of both DPDCH and DPCCH as well as their raw BERs which is calculated before the turbo decoder. Furthermore the *Block Error Rate* (BLER) is presented as it is an important measure considering frame re-transmissions.

3.3.1 Saleh Results

In Figures 3.15 and 3.16 we have evaluated the system performance of DPDCH and DPCCH respectively considering their raw bit error probability and their actual BER. The system has simulated 10 superframes, which means 720 frames translating into 141120 bits per physical channel. For a better confidence we have run 20 simulations and acquired the average performance.

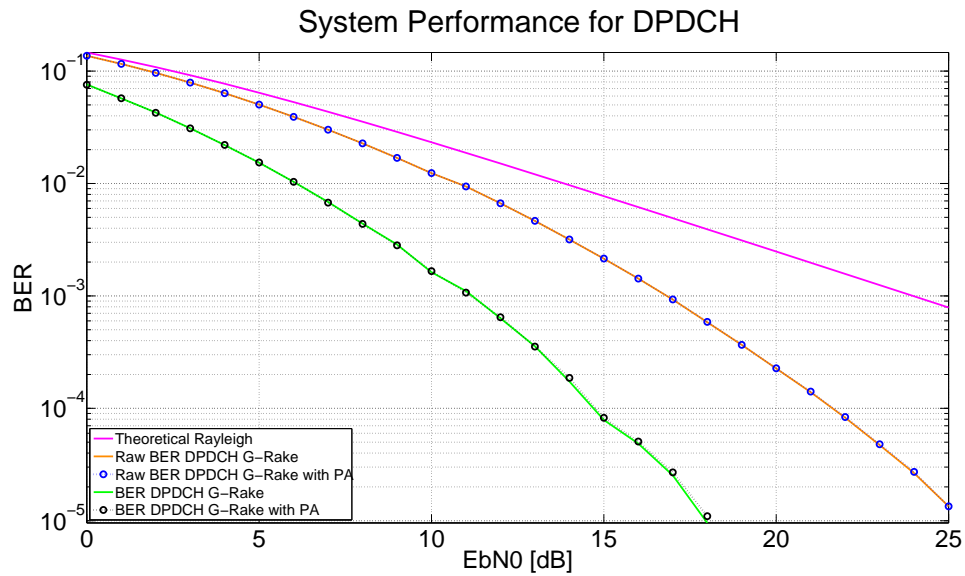


Figure 3.15: Saleh model performance for DPDCH. The raw BER is before the turbo decoder whereas the BER is the performance after the turbo decoder.

From the results one can understand clearly that from the Saleh model phase distortion there is no system performance degradation considering both before and after the turbo decoder. Both physical channels are equally not affected when the HS-channels are added on top.

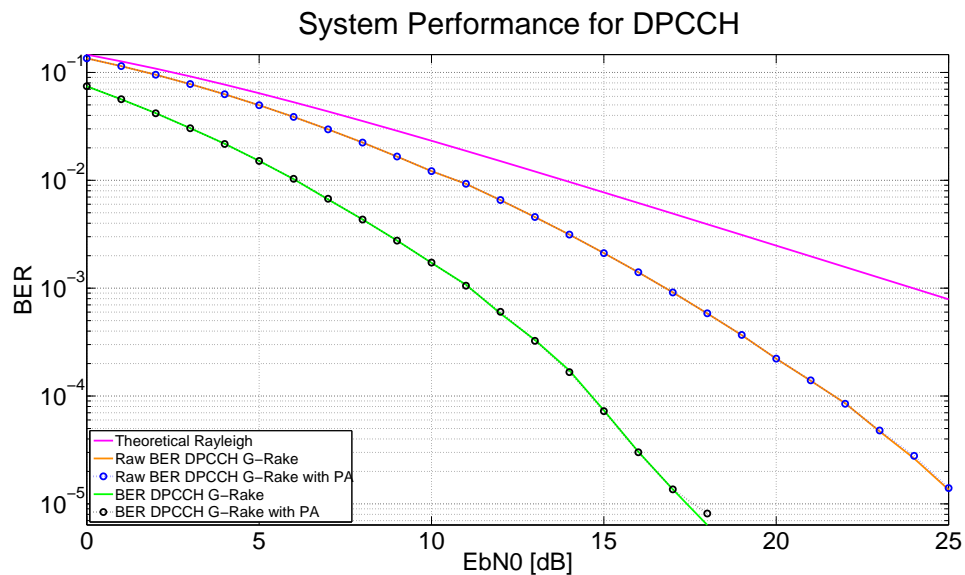


Figure 3.16: Saleh model performance for DPCCH. The raw BER is before the turbo decoder whereas the BER is the performance after the turbo decoder.

A further understanding of the reason why the system performance does not change can be seen in Figure 3.17. In this figure the received signal's constellation can be observed in terms of different E_b/N_0 , where it is very clear that with and without power amplifier there are slight changes of the signal. That happens because the channel estimator is able to remove the constant value of phase distortion that the PA introduces and then just very small phase changes remain in the signal. Those small changes can be mostly seen on the outer values of the signal where the distortion might be a little bit bigger due to the signal amplitude inserted to the PA.

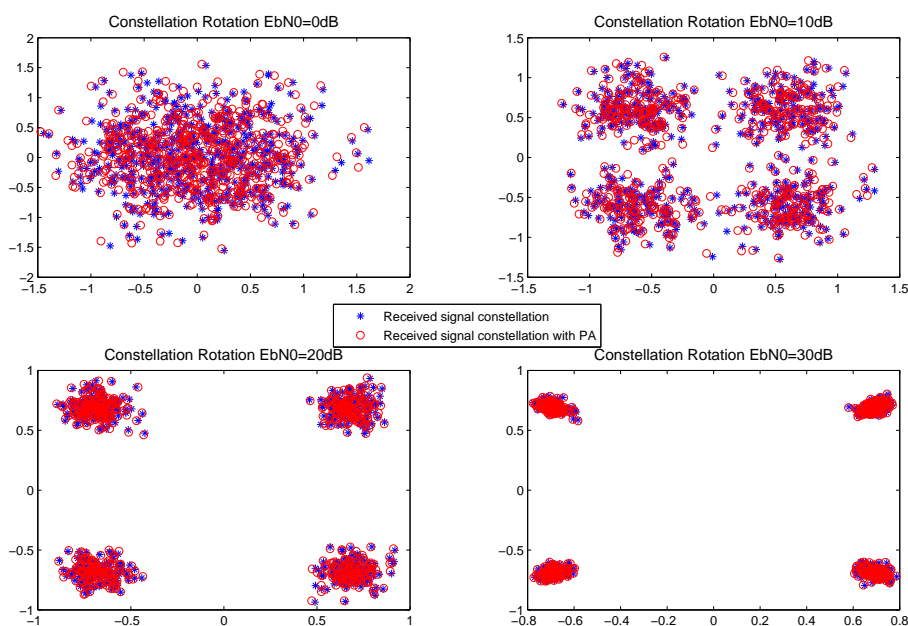


Figure 3.17: Saleh model received signal constellation rotation. The blue star stands for signal without PA's effect, and the red circle stands for signal with PA's phase distortion.

Block error rate is a very important metric due to the fact that on it the retransmissions are based and therefore the whole system performance. From Figure 3.18, it is clear that the system performance is the same without any clear effects due to those small phase distortions from the PA.

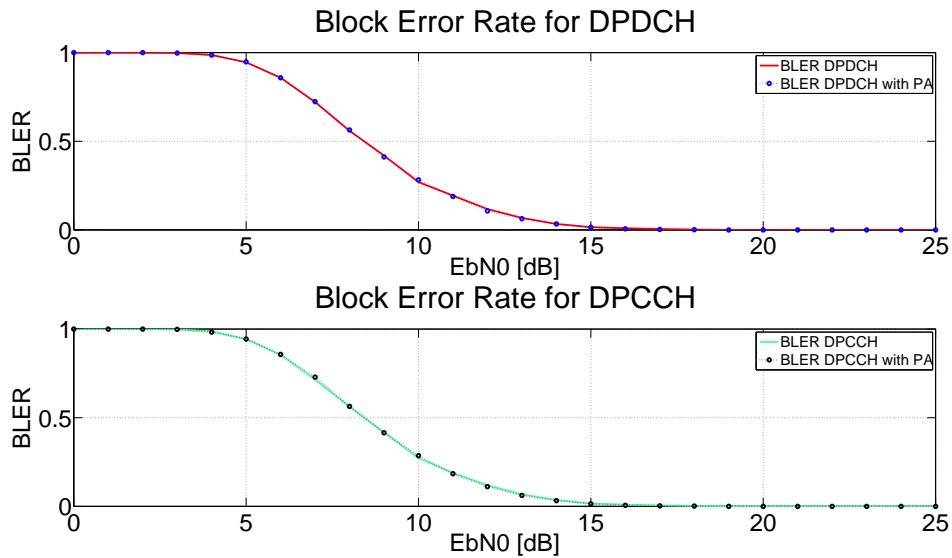


Figure 3.18: Saleh model block bit error rate

3.3.2 Polynomial Results

As mentioned previously, in order to approach the reality even more we fit a polynomial on real measurements in order for us to evaluate even better the results of such a phase discontinuity. The BER performance and the raw BER can be seen in Figures 3.19 and 3.20.

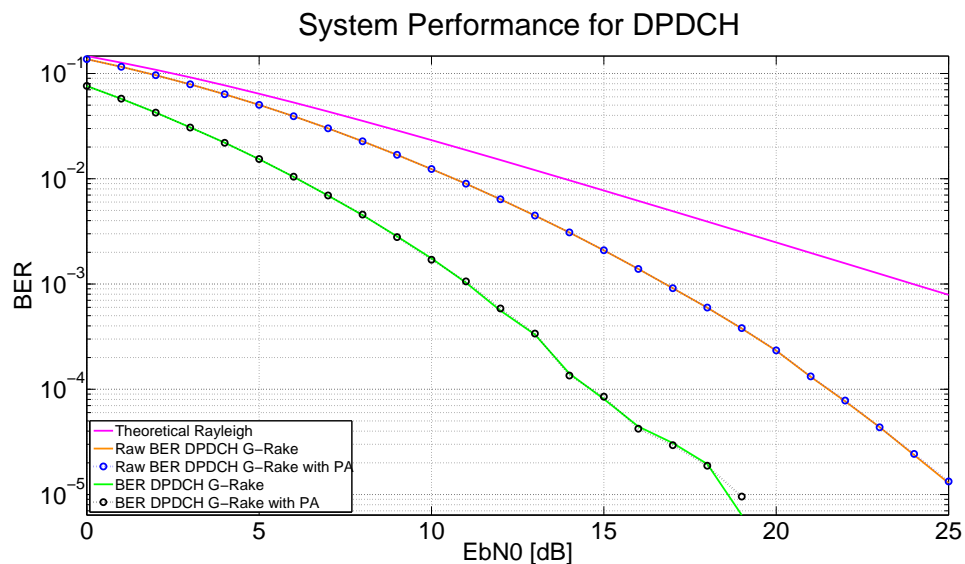


Figure 3.19: Polynomial model performance for DPDCH. The raw BER is before the turbo decoder whereas the BER is the performance after the turbo decoder.

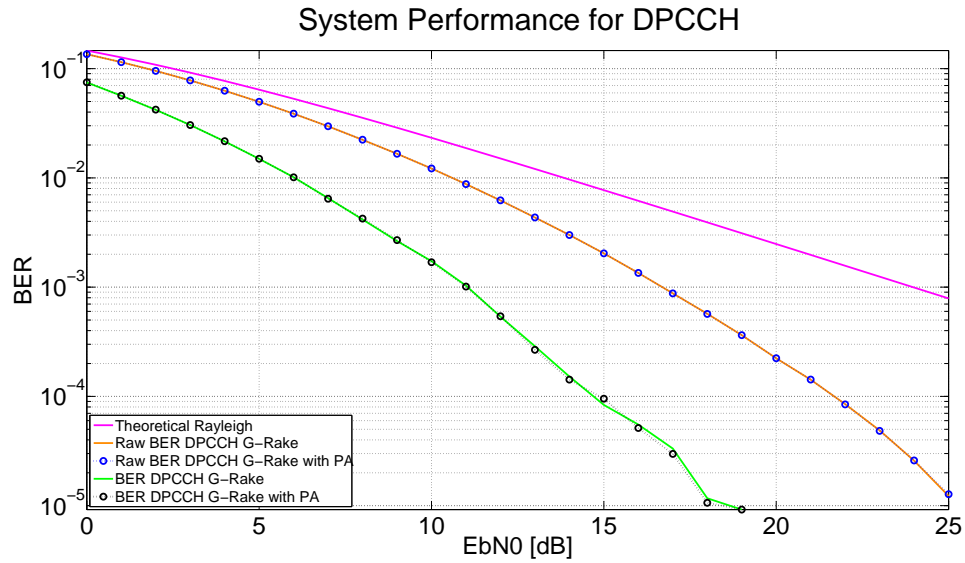


Figure 3.20: Polynomial model performance for DPCCH. The raw BER is before the turbo decoder whereas the BER is the performance after the turbo decoder.

Once again on Figure 3.21 it is obvious that the constant value of the phase rotation is removed and only small values of phase distortion are present in the signal with the help of our channel estimator.

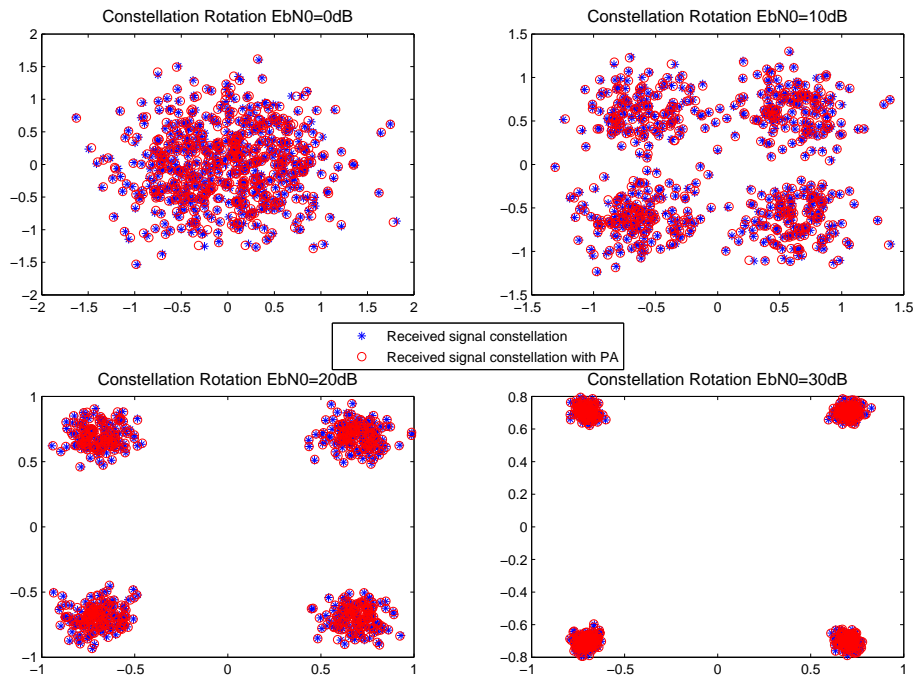


Figure 3.21: Polynomial model received signal constellation rotation. The blue start stands for signal without PA’s effect, and the red circle stands for signal with PA’s phase distortion.

As expected, for an almost equal range of phase distortion as modelled in previous sections, it is again anticipated that the system will be able to cope with, in an equivalent way, with the phase distortion. Thus, there is no degradation of the performance. The same outcome can be observed from the BLER of the polynomial model as can be seen in Figure 3.22.

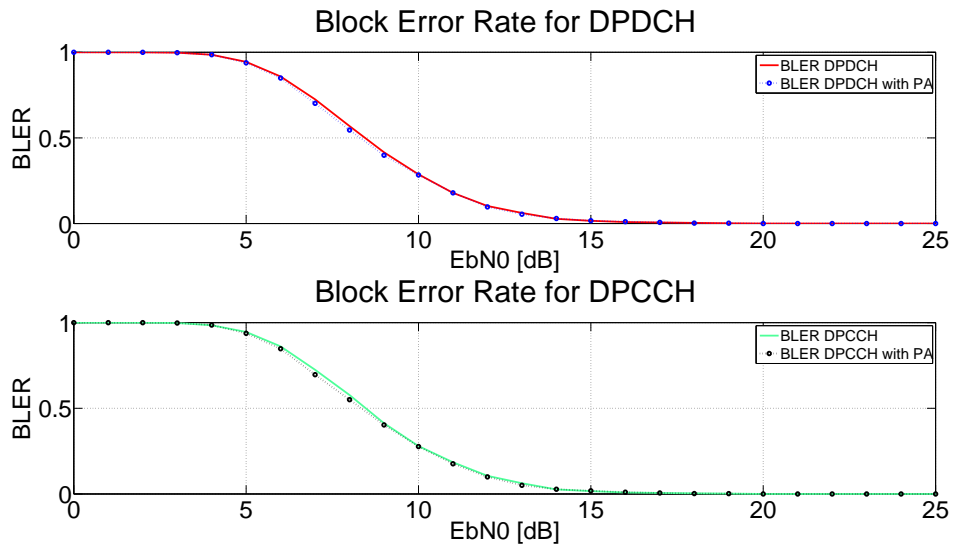


Figure 3.22: Polynomial model block bit error rate

4

Conclusions

This study was set out to explore the concept of power amplification on an uplink WCDMA link. More specifically the impact that such a power amplification can introduce to the system. Such a non-perfect system as a PA provides the transmitting link with distortion considering the phase of the signal that is sent through the channel. Therefore, such a phase distortion could be a good candidate to provide BER degradation. The literature contains a wide variety of knowledge about power amplifiers but on the subject of distortion due to phase discontinuity it is inconclusive of these two questions below that the current study sought to answer.

1. How much is the BER degradation due to the PA phase distortion?
2. In case there is BER degradation, then how much of it can the standardised WCDMA system accept before measures should be taken?

In order to answer those two questions correctly a realistic WCDMA system would be needed to test such behaviours. For that cause, an end-to-end simulator was built in order to capture even the smaller factors of the WCDMA uplink, so that the results could be realistic and therefore provide good answers to our questions.

The answer to a more generic question as "Is there any BER degradation due to the PA phase distortion?" is a definite yes. And that can be both understood through a theoretical approach where the symbol due to the rotation approaches the decision regions as well as the simulation results from which slight changes on the BER happened. Nevertheless, the answer to our real question is that the system performance is very slightly affected. That of course can be explained with the quality of the PAs that are used in the uplink and the robustness of the WCDMA system in total.

Considering only the phase distortion of the PA, then low degrees of distortion can be seen as minor changes regarding the thresholds of a QPSK modulation even without the robustness of WCDMA performance protection techniques. The thresholds of such a modulation are very much higher than the phase distortion added and that results in a system having almost exactly the same performance as without it. Having said that,

we had already answered the second question, as the system which has been created to work on such performances towards BER will continue without any further problems. The system has provided us with results within its current configuration. On the other hand, the world demand about more higher bit rate might actually change the system in such a way that power levels might be forced higher than before. In such case the PA behaviour shall be different and that difference will also produce different distortion to the phase. Furthermore, there are higher order of modulations such as 16-QAM or higher. In addition to that if multiple antenna technology is to be implemented then there should be different behaviours that the current thesis work has not explored. Then the research should be again conducted about the renewed versions of amplifiers or any other considerable changes in the system that might push the amplifier in such a region that the phase distortions produced will not be able to be accounted for.

A

RAKE Receiver

The RAKE receiver mathematical expressions are mentioned as described in [23]. In the receiver, the received signal after multipath fading is

$$y(m) = \underbrace{h(0)x(m)}_{\text{Current Symbol}} + \underbrace{h(1)x(m-1) + h(2)x(m-2) + \cdots + h(L-1)x(m-(L-1))}_{\text{L-1 past symbols}},$$

where $h(L-1)$ is the channel coefficient for the symbol $x(m-(L-1))$ and $x(m)$ is the m^{th} transmitting symbol.

For WCDMA signal, we obtain the transmitting symbol by multiplying the symbol of the user with the spreading code as shown in Eq. (A.1).

$$x(m) = s_0 c_0(m), \quad (\text{A.1})$$

where s_0 is the user-0's symbol and $c_0(m)$ is the spreading code for user-0 for the m^{th} symbol.

Then as in Eq. (A.2) if $x(m)$ passes through the multipath channel, we can receive the signal

$$y(m) = \sum_{m=0}^{L-1} h(d)x(m-d) + u(m), \quad (\text{A.2})$$

where $u(m)$ is the noise that symbol $x(m)$ gets and $h(d)$ are the channel coefficients for tap d .

If we substitute Eq. (A.1) to (A.2), then we get

$$y(m) = \sum_{m=0}^{L-1} h(d)s_0 c_0(m-d) + u(m). \quad (\text{A.3})$$

At the receiver we correlate the received signal of the user and the corresponding spreading code of the user.

For path 0:

$$r(0) = \frac{1}{N} \sum_{m=0}^{N-1} y(m)c_0(m). \quad (\text{A.4})$$

Substitute Eq. (A.3) to (A.4), then

$$r(0) = \frac{1}{N} \sum_{m=0}^{N-1} \sum_{m=0}^{L-1} h(d)s_0c_0(m-d)c_0(m) + \frac{1}{N} \sum_{m=0}^{N-1} u(m)c_0(m).$$

For the path 0, $d = 0$ so

$$r(0) = \frac{1}{N} \sum_{m=0}^{N-1} \sum_{m=0}^{L-1} h(0)s_0c_0(m)c_0(m) + \frac{1}{N} \sum_{m=0}^{N-1} u(m)c_0(m),$$

as $c_0(m)^2 = 1$ and define $\tilde{u}(0) = \frac{\sigma_u^2}{N}$, we can get

$$\begin{aligned} r(0) &= \frac{1}{N} \sum_{m=0}^{N-1} \sum_{m=0}^{L-1} h(0)s_0 + \frac{1}{N} \sum_{m=0}^{N-1} u(m)c_0(m) \\ &= s_0h(0) + \tilde{u}(0). \end{aligned} \quad (\text{A.5})$$

For the next path, the output of finger is the similar as path 0:

$$\begin{aligned} r(1) &= \frac{1}{N} \sum_{m=0}^{N-1} y(m)c_0(m-1) \\ &= \frac{1}{N} \sum_{m=0}^{N-1} \sum_{m=0}^{L-1} h(d)s_0c_0(m-d)c_0(m-1) + \frac{1}{N} \sum_{m=0}^{N-1} u(m)c_0(m-1) \\ &= \frac{1}{N} \sum_{m=0}^{N-1} \sum_{m=0}^{L-1} h(1)s_0c_0(m-1)c_0(m-1) + \frac{1}{N} \sum_{m=0}^{N-1} u(m)c_0(m-1) \\ &= s_0h(1) + \tilde{u}(1). \end{aligned} \quad (\text{A.6})$$

Similarly we can correlate up all the L paths

$$\begin{cases} r(0) &= s_0h(0) + \tilde{u}(0) \\ r(1) &= s_0h(1) + \tilde{u}(1) \\ \vdots & \\ r(L-1) &= s_0h(L-1) + \tilde{u}(L-1). \end{cases}$$

From above, we can conclude the expression for path d as

$$\Rightarrow r(d) = s_0h(d) + \tilde{u}(d), \quad (\text{A.7})$$

$$\begin{bmatrix} r(0) \\ r(1) \\ r(2) \\ \vdots \\ r(L-1) \end{bmatrix} = s_0 \begin{bmatrix} h(0) \\ h(1) \\ h(2) \\ \vdots \\ h(L-1) \end{bmatrix} + \begin{bmatrix} \tilde{u}(0) \\ \tilde{u}(1) \\ \tilde{u}(2) \\ \vdots \\ \tilde{u}(L-1) \end{bmatrix}. \quad (\text{A.8})$$

Using vector notation, the signal after receiver is

$$\mathbf{r} = s_0 \mathbf{h} + \tilde{\mathbf{u}}. \quad (\text{A.9})$$

The same symbol is received by different paths thus gaining multipath diversity. The vector \mathbf{h} comprises the channel gains from multipath diversity, and the vector $\tilde{\mathbf{u}}$ consists of the noise that affects the signals at every path.

Then using linear combiner to maximise the SNR

$$r = w_0^* r(0) + w_1^* r(1) + \cdots + w_{L-1}^* r(L-1), \quad (\text{A.10})$$

where $w = \frac{h}{\|h\|}$, and $\mathbf{w} = \frac{\mathbf{h}}{\|h\|}$ is the finger weights.

Combining this with the Eq. (A.9) the received signal become

$$\begin{aligned} r &= \mathbf{w}^H \mathbf{r} \\ &= \frac{\mathbf{h}^H}{\|h\|} \mathbf{r} \\ &= \frac{\mathbf{h}^H}{\|h\|} (s_0 \mathbf{h} + \tilde{\mathbf{u}}) \\ &= \underbrace{\|h\| s_0}_{\text{Signal}} + \underbrace{\frac{\mathbf{h}^H}{\|h\|} \tilde{\mathbf{u}}}_{\text{Noise}}. \end{aligned} \quad (\text{A.11})$$

Now the power of the signal is $\|h\|^2 P_0$ and the power of the noise is $\frac{\sigma_u^2}{N}$, where the P_0 is the power of the input signal s_0 .

Then the SNR is

$$SNR = \frac{\|h\|^2 P_0}{\frac{\sigma_u^2}{N}} = \frac{\|h\|^2 P_0 N}{\sigma_u^2}. \quad (\text{A.12})$$

Bibliography

- [1] A. S. Sedra, K. C. Smith, *Microelectronic Circuits*, Oxford University Press, 2009.
- [2] K. M. Gharaibeh, *Nonlinear Distortion in Wireless Systems: Modeling and Simulation with MATLAB*, Wiley, 2011.
- [3] V. T. Andrea Conti, Davide Dardari, *An Analytical Framework for CDMA Systems With a Nonlinear Amplifier and AWGN*, *IEEE TRANSACTIONS ON COMMUNICATIONS VOL 50*.
- [4] R. G. Seng-Woon Chen, William Panton, *Effects of Nonlinear Distortion on CDMA Communication Systems*, *IEEE Transactions on Microwave Theory and Techniques, VOL 44*.
- [5] M. E.-T. Tarek K. Helaly, Richard M. Dansereau, *Analysis of BER Performance in Presence of Nonlinear Distortion Due to PD-HPA in Downlink DS-CDMA Signal*, *IEEE COMMUNICATIONS LETTER. VOL 14*.
- [6] H. Holma, A. Toskala, *WCDMA For UMTS: Radio Access For Third Generation Mobile Communications*, Wiley, 2001.
- [7] T. Nakamura, K. Ohbuchi, Y. Tajima, T. Yano, Y. Tanaka, *Radio Access Technologies and Signaling Scheme in W-CDMA System*, *Fujitsu Scientific and Technical Journal 72 (2002) 149*.
- [8] J. Korhonen, *Introduction to 3G Mobile Communicaitons*, Artech House, 2001.
- [9] G. E. Bottomley, D. A. Cairns, C. Cozzo, T. L. Fulghum, A. S. Khayrallah, P. Lindell, M. Sundelin, Y.-P. E. Wang, *Advanced receivers for WCDMA terminal platforms and base stations*, *Ericsson Review*.
- [10] J. G. Proakis, M. Salehi, *Communication Systems Engineering*, Prentice Hall, 1994.
- [11] C. Berrou, A. Glavieux, P. Thitimajshima, *Near Shannon Limit Error - Correcting Coding and Decoding : Turbo-Codes (1)*, *IEEE Journal on Selected Areas in Communications*.

- [12] E. Dahlman, S. Parkvall, J. Sköld, P. Beming, 3G Evolution: HSPA and LTE for Mobile Broadband, Academic Press, 2007.
- [13] E. H. Dinan, B. Jabbari, Spreading Codes for Direct Sequence CDMA and Wideband CDMA Cellular Networks, IEEE Communications Magazine 36 (1998) 48–54.
- [14] A. Richardson, WCDMA Design Handbook, Cambridge University Press, 2011.
- [15] ETSI, Universal Mobile Telecommunications System (UMTS); Selection procedures for the choice of radio transmission technologies of the UMTS (UMTS 30.03 version 3.2.0), ETSI, TR 101 112 V3.2.0. (1998-04).
- [16] T. S. Rappaport, Wireless Communications: Principles and Practice, Prentice Hall, 2002.
- [17] G. E. Bottomley, T. Ottosson, Y.-P. E. Wang, A Generalized Rake Receiver For DS-CDMA Systems, IEEE Journal on Selected Areas in Communications 2.
- [18] B. Razavi, RF Microelectronics, Prentice Hall, 2012.
- [19] S. C. Cripps, RF power amplifiers for Wireless Communications, Artec House, 2006.
- [20] L. C. N. Telmo R. Cunha, Pedro M. Cabral, Characterizing Power Amplifier Static AM/PM with Spectrum Analyzer Measurements.
- [21] R. W. Gerhard, Nonlinear Behavior And Digital Phase Predistortion Of Outphasing Power Amplifiers.
- [22] S. A. V. D. GEER, Least Squares Estimation, Encyclopedia of Statistics in Behavioral Science 15.
- [23] A. K. Jagannatham, Advanced 3G and 4G Wireless Mobile Communications, Department of Electronics and Communication Engineering, IIT Kanpur.